Approach to universality in axisymmetric bubble pinch-off

Stephan Gekle, Jacco H. Snoeijer, Detlef Lohse, and Devaraj van der Meer
Department of Applied Physics and J.M. Burgers Centre for Fluid Dynamics, University of Twente, P.O. Box 217, 7500 AE Enschede, The Netherlands

(Received 15 April 2009; revised manuscript received 19 June 2009; published 4 September 2009)

The pinch-off of an axisymmetric air bubble surrounded by an inviscid fluid is compared in four physical realizations: (i) cavity collapse in the wake of an impacting disk, (ii) gas bubbles injected through a small orifice, (iii) bubble rupture in a straining flow, and (iv) a bubble with an initially necked shape. Our boundary-integral simulations suggest that all systems eventually follow the universal behavior characterized by slowly varying exponents predicted by J. Eggers *et al.* [Phys. Rev. Lett. **98**, 094502 (2007)]. However, the time scale for the onset of this final regime is found to vary by orders of magnitude depending on the system in question. While for the impacting disk it is well in the millisecond range, for the gas injection needle universal behavior sets in only a few microseconds before pinch-off. These findings reconcile the different views expressed in recent literature about the universal nature of bubble pinch-off.

DOI: 10.1103/PhysRevE.80.036305 PACS number(s): 47.55.df, 47.11.Hj, 47.15.km

The precise nature of axisymmetric bubble collapse in a low-viscosity fluid has been a subject of controversy over the last years. Such a collapse may be initiated by a variety of different forces (e.g., surface tension, hydrostatic pressure, and external flows). In a later stage, however, it is only the requirement of mass conservation that forces the liquid to accelerate more and more as the shrinking bubble neck closes in on the axis of symmetry. This purely inertial nature of the final collapse motivated the first hypotheses about the universality of the final collapse regime [1,2]. A simple power law was predicted with the neck radius scaling as the square root of the time remaining until the pinch-off singularity. Neither numerically nor experimentally could this behavior be confirmed. Instead, for different systems and initial conditions a variety of scaling exponents all slightly above 1/2 have been obtained [3–10] leading to doubts about the universal nature of bubble collapse.

Recently, the idea of universality has been revived in [11,12] which suggested an intricate coupling between the radial and the axial length scales. The authors of [12] explicitly predict the existence of a final universal regime which however is no longer a simple power law, but characterized by a local exponent that slowly varies in time. The value of 1/2 is recovered in the asymptotic limit infinitesimally close to pinch-off. According to this theory the variety of observed exponents corresponds to different time averages of this local exponent. Note that this is different from the universality as observed, for example, in the pinch-off of a drop [13] where the behavior of the neck radius can be described by a scaling law whose universal exponent remains constant in time. With the exception of the rather idealized system used in [12], this universality has thus far never been directly observed in neither experiments nor simulations.

In the present work we aim to reconcile the different views about universality in axisymmetric bubble pinch-off expressed over the last years. The key aspect is that we examine in detail how and when different physical realizations of bubble pinch-off reach the universal regime. We present detailed numerical simulations which are able to follow the neck evolution over more than 12 decades in time even for complex realistic systems. With these we demonstrate that all systems that have recently been studied in the context of bubble pinch-off eventually follow the same universal behavior predicted in [12]. The time scale on which universality is reached, however, varies enormously: for an impacting disk [4,14] universality can be observed during several milliseconds prior to pinch-off and thus on a time scale, which is experimentally accessible. However, for gas bubbles injected through a small needle [1,2,5–10,15–17], universality sets in only a few microseconds (or even less, depending on the precise initial conditions) before pinch-off. This may well be the reason why universality has thus far never been observed even in very precise gas injection experiments and why noninertial effects such as surface tension have been claimed to play a dominant role in this geometry [9,10]. By specifying the onset times of universality, our work thus provides a solid basis to which onset times of nonuniversal disturbance effects such as viscosity, air flow, or nonaxisymmetry can be compared in order to assess whether or not a given system would in reality exhibit such a universal behavior.

Four different physical systems have been reported in the literature on bubble pinch-off, numerically and experimentally, and will be compared in this work:

(i) *Impacting disk*. The bubble is created by the impact of a circular disk on a liquid surface [4,14] as shown in Fig. 1(i). Upon impact an axisymmetric air cavity forms and eventually pinches off halfway down the cavity under the influence of hydrostatic pressure. Immediately after pinch-off, the ejection of a violent jet can be observed whose formation however is not caused by the singularity alone [18] as one might expect. Since surface tension is negligible [4,14,18] the only relevant control parameter is the Froude number $\mathrm{Fr}=V_0^2/gR_0$ with the impact velocity V_0, gravity g, and the disk radius R_0. In the data reported here the disk radius varies between 1 and 3 cm and the impact velocity ranges from 1 to 20 m/s.

(ii) *Gas injection through an orifice*. A small needle sticks through the bottom of a quiescent liquid pool [1,2,5–10,15–17] as illustrated in Fig. 1(ii). A pressure reservoir connected to the needle slowly pushes a gas bubble out of the needle's orifice. The bubble then rises under the influ-

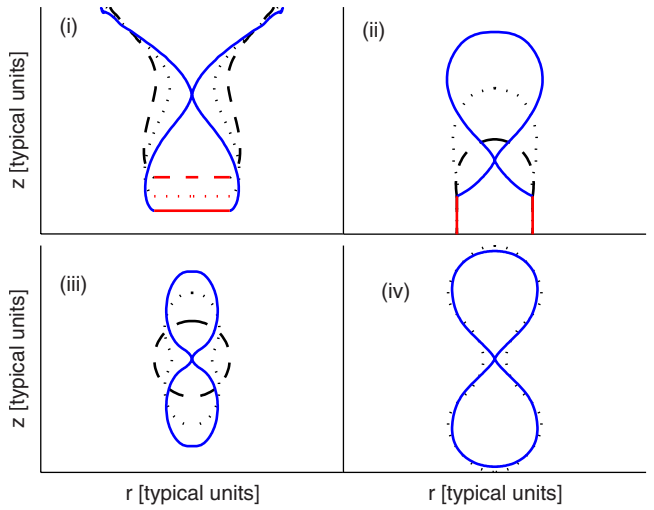

FIG. 1. (Color online) Illustration of the bubble collapse in the four different systems: (i) impacting disk, (ii) gas injection through a needle orifice, (iii) bubble in a straining flow, and (iv) initially necked bubble. Solid blue lines correspond to the free surface at pinch-off, while dashed and dotted black lines represent earlier bubble shapes. The disk and the needle are depicted in red (light gray).

ence of buoyancy. When the air thread between the orifice and the main bubble becomes long enough, surface tension causes the thinning of the neck, which eventually leads to the pinch-off of the bubble. We present data for three sample configurations A, B, and C corresponding to Figs. 4, 10, and 6 of [2], respectively, and characterized by Weber numbers $\mathrm{We}_{\mathrm{A,B,C}}=0.007$, 36 and 173, respectively. [Here, We $=\rho Q^2/(\pi^2 a^3 \sigma)$ with water density ρ, gas flow rate Q, needle radius a, and surface tension σ].

(iii) *Bubble in a straining flow*. The initially spherical bubble collapses due to a surrounding hyperbolic straining flow [3,11,19,20] [see Fig. 1(iii)].

(iv) *Initially necked bubble*. Surface tension causes the pinch-off of a bubble starting off with an initially already pronounced neck [12] as illustrated in Fig. 1(iv).

In all systems we consider the idealized inviscid axisymmetric bubble pinch-off neglecting the influence of the inner gas dynamics [3,8–10,20–23], viscosity [6,9,10,15], and nonaxisymmetric perturbations [16,17]. For our numerical investigations we employ an axisymmetric boundary-integral (BI) code similar to the one described in [14] which has shown a very good agreement with experiments of system (i) for various impact geometries [4,14,24]. The validity of our implementation for the other systems is verified by comparison with the bubble shapes from various earlier works [2,12,19]. Some details about the simulation parameters are given in the EPAPS document [25].

In a first approach to an analytical description of bubble collapse, the bubble shape can be approximated as an infinitely long cylinder (neglecting axial velocities) which yields a two-dimensional version of the well-known Rayleigh equation [2–4,11,15] for the neck radius r_0

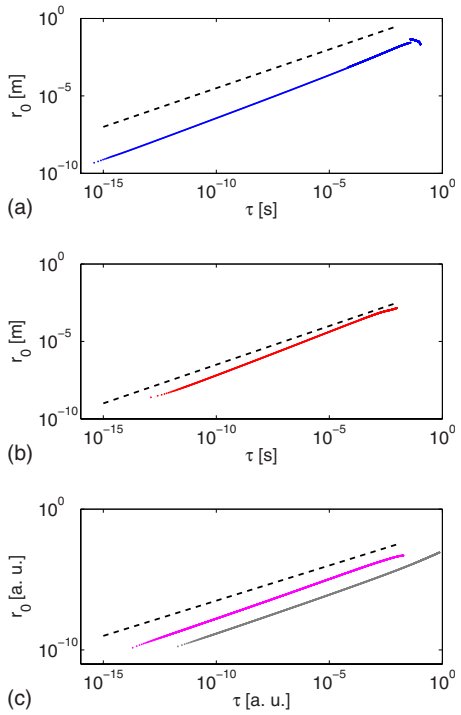

FIG. 2. (Color online) "Classical" plot of the neck radius versus the time to pinch-off (a) for system (i) with Fr=5.1 ($R_0=2$ cm, $V_0=1$ m/s), (b) for system (ii) in setup A, and (c) for systems (iii) and (iv) shown in dark gray (lower line) and magenta (upper line), respectively. The dashed line represents a slope of 1/2.

$$\frac{d(r_0\dot{r}_0)}{dt}\ln\frac{r_0}{R_\infty}+\frac{1}{2}\dot{r}_0^2=\frac{F}{\rho}. \tag{1}$$

Here, ρ is the liquid density, F represents the pressure force initiating the collapse, and overdots denote the derivative with respect to time t. R_∞ is a cutoff radius required to saturate the pressure at large distances. Assuming a constant R_∞ leads to the neck radius r_0 shrinking as a power law (possibly with logarithmic corrections [3,4,11]) with exponent 1/2 as a function of the time to pinch-off $\tau=t_c-t$, where t_c is the closure time. At first sight, this expectation seems to be very well confirmed for all four systems by the lines in Fig. 2 which to the naked eye appear perfectly straight over more than 12 decades. The slope which corresponds to the scaling exponent is slightly larger than 1/2, in agreement with previous experiments and simulations which have reported exponents between 0.5 and 0.6 [3–6,8–11,15].

A more detailed look at the local exponent, defined as the slope in Fig. 2, $\alpha(\tau)=\partial \ln r_0/\partial \ln \tau$, reveals that the behavior of the neck radius cannot be described by a simple power law. The local exponent α varies during the approach to pinch-off [12]. In fact, the relevant equation for the time dependence of α in [12] can be derived directly from Eq. (1) by letting $R_\infty=2\sqrt{r_0 r_c}$. Here, r_c is the local axial radius of curvature (see Fig. 3). The combination $\sqrt{r_0 r_c}$ is the scale by which the axial coordinate has to be rescaled in order to collapse neck profiles at different times when rescaling radial coordinates by r_0 [4,6,26]. This leads to the aspect ratio of the cavity naturally being defined as $\gamma=r_0/\sqrt{r_0 r_c}$. With the

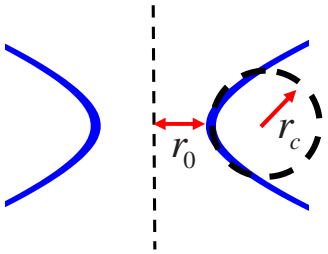

FIG. 3. (Color online) Illustration of the cavity surface, the minimal neck radius r_0, and the local radius of curvature r_c.

above substitutions and working in the limit of vanishing F, i.e., in the regime where the influence of the driving force has become subdominant, we obtain from Eq. (1)

$$\left(-\frac{d\alpha}{d\ln\tau}+\alpha-2\alpha^2\right)\ln\left(\frac{4}{\gamma^2}\right)=-\alpha^2, \tag{2}$$

which is exactly identical to Eq. (4) in [12] (being $\Gamma_1=8$ [27] and $a_0''=2\gamma^2$ in the original notation). Equation (2) with the $d\alpha/d\ln\tau$ term neglected due to the slow variation in α [28] represents the universal regime where the only driving is provided by inertia and all external forces have become negligible. We will now proceed to compare the approach of the different systems (i)–(iv) to this universal curve. Equation (2) with the above approximation suggests to represent α not as a function of time to pinch-off τ, but instead as a function of the aspect ratio γ. Since there is a one-to-one correspondence between τ and γ shown in Fig. 4, we can use the aspect ratio γ as a universal "clock" replacing the time to pinch-off τ [27]. Note that $\gamma\to 0$ as $\tau\to 0$, meaning that the cavity becomes more and more slender [6,11]. Another motivation to use γ instead of τ is that Eq. (2) is invariant under a rescaling of time $\tau\to\beta\tau$ reflecting an arbitrariness of the time coordinate in this problem. The aspect ratio γ does not possess this arbitrariness.

One of the key points to address is if and how this behavior can be observed experimentally. Besides the obvious difficulty of obtaining a sufficient number of decades to observe the slow variation in the local exponent, the crucial question is at what time (before pinch-off) does the system exhibit a universal behavior? This is crucial because, first, the duration of the universal regime needs to be within the time resolution of the experimental equipment. And second, the onset of

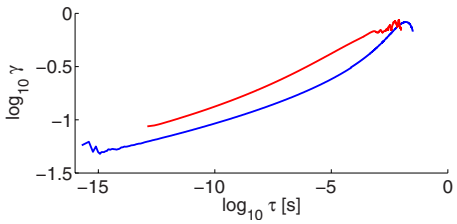

FIG. 4. (Color online) The aspect ratio γ plotted as a function of the time to pinch-off τ for system (i) with Fr=5.1 (blue lower line) as well as system (ii) in setup A (red upper line). This shows that one can use γ instead of τ as a measure for the approach to pinch-off.

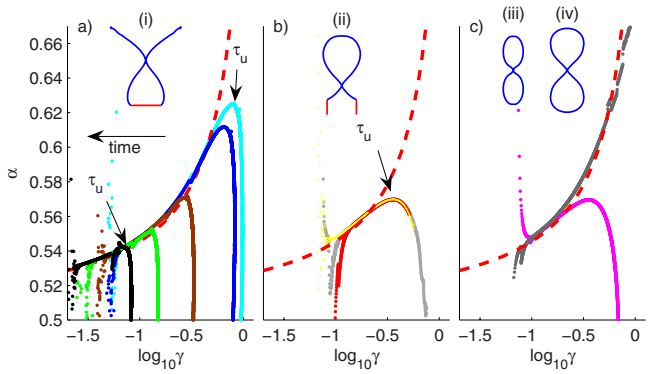

FIG. 5. (Color online) (a) The local exponent α as a function of the aspect ratio γ for system (i) with Fr=3.4 (cyan, rightmost curve), Fr=5.1 (blue curve), Fr=46 (brown curve), Fr=500 (green curve), and Fr=4000 (black, leftmost curve). After an initial transient all curves follow the same universal regime. The dashed line is Eq. (2). The local maxima correspond roughly to the start of the universal regime. (b) The local exponent for system (ii) in the three configurations: A (red, dark gray curve), B (gray curve), and C (yellow, very light gray curve). All curves A–C lie practically on top of each other. (c) The local exponent for system (iii) in dark gray (upper curve) and system (iv) in magenta (light gray, lower curve) follows the same universal behavior close to pinch-off. Small jumps in the data are due to the crossover between different node positioning algorithms employed in the initial and the final stages of the simulation (see EPAPS document [25]), while the deviation of the numerical data away from the universal curve at the very end stems from the uncertainty in determining the exact time of closure.

universality needs to happen before other effects such as air flow, viscosity, nonaxisymmetric instabilities, etc. unavoidably destroy the purely inertial regime. We will now provide those time scales for the various systems based on numerical BI simulations which do not have these limitations.

We start by considering the impacting disk system (i) in Fig. 5(a). It is evident that the data for all values of the control parameter follow—after some initial transient—the same universal curve in excellent agreement with Eq. (2). Our data thus confirm the existence of a universal regime as predicted in [12]. Since from Fig. 5 the closure time cannot be determined in a straightforward manner, the closure time has been estimated by fitting straight lines in plots like in Fig. 2. As this procedure is not exact due to the time dependence of the local scaling exponent, it leads to a deviation of the numerical data from the universal curve in Fig. 5 toward the very end which however is merely an artifact of the uncertainty in the exact closure time.

Figure 5(a) further gives us a good measure at what aspect ratio the universal regime is attained: approximately after passing their respective local maxima, all curves follow the same behavior. The aspect ratio of this maximum can then easily be related to the physical time before pinch-off τ_u using Fig. 4. We find $\tau_u\approx 6$ ms and $\tau_u\approx 1$ ms for Fr=3.4 and Fr=4000, respectively. That the high Froude case reaches universality later can be intuitively understood: at high Froude the cavity closes deeper and therefore the hydrostatic driving pressure is larger and its effects on the neck

dynamics can be felt longer. It is remarkable nevertheless that the duration of the universal regime changes only by a factor of less than 10, while the corresponding control parameter varies over three orders of magnitude. At the same time both values are easily within experimentally accessible time scales.

We now compare this to system (ii), the bubble injection through a small needle in Fig. 5(b). While also this system clearly exhibits universal behavior, the approach to the universal regime is much less abrupt than in system (i). Due to this more gradual approach, it is difficult to specify precisely the time when universality is reached for the gas injection needle. We thus choose to keep our previous definition of τ_u being the time corresponding to the local maximum in Fig. 5(b). This gives a good upper bound for the time when universality sets in. Surprisingly, we find even these times to be on the order of 5 μs in case A, 60 ns in case C, and as low as 10 ns in case B, respectively [29]. Thus, the duration of the universal regime in the needle setup is dramatically (by at least three orders of magnitude) shorter than for the impacting disk. This may well explain why, besides possible disturbing effects (viscosity, gas flow, and nonaxisymmetry), an observation of the universal regime has thus far never been reported in the literature on this widely used system.

Figure 5(c) confirms that also systems (iii) and (iv) follow the universal regime. System (iii) does so even over the entire plotted range. Both are somewhat idealized systems for which we are not aware of any experimental investigations regarding the approach to pinch-off. Without relevant length and time scales, it is impossible to specify the physical time to universality in these cases.

The different behaviors of the individual systems can intuitively be understood as follows. System (iii) contains no external driving force other than liquid inertia, which makes it the ideal system to compare with Eq. (2). Indeed, this entirely inertial system follows the universal regime over the widest range in aspect ratios of all systems studied. Similarly, due to the relatively large dimensions of the collapsing cavity in system (i), a correspondingly large amount of inertia is introduced into the system which consequently follows the universal regime also for a rather long time. On the other hand, the two systems where pinch-off is initiated by surface tension, systems (ii) and (iv), contain little inertia and thus approach the universal regime only relatively late and in a similar fashion.

To make the above arguments more quantitative, we realize that the universal regime sets in when the inertial driving of the collapse becomes dominant over the external driving force. This can be expressed by a local balance between inertia and the respective driving force. For system (i) the driving force is the hydrostatic pressure and the relevant parameter is thus the local Froude number $\mathrm{Fr}_{\mathrm{local}}=\dot{r}_0^2/(gz_c)$ with gravity g and z_c as the depth below the surface where the cavity eventually closes. For system (ii) the local Weber number $\mathrm{We}_{\mathrm{local}}=\rho\dot{r}_0^2 r_0/\sigma$ (with density ρ and surface tension σ of water) gives the balance between inertia and surface tension as the relevant driving force. The duration of the universal regime can then be estimated as the time before pinch-off when these local quantities become of order unity. Figure 6 shows the local Froude and Weber numbers as functions of time to pinch-off τ for a number of representative cases of systems (i) and (ii), respectively. One can clearly appreciate that $\mathrm{We}_{\mathrm{local}}$ for the needle system becomes unity later than $\mathrm{Fr}_{\mathrm{local}}$ for the impacting disk. This explains the large discrepancy in τ_u for the two systems.

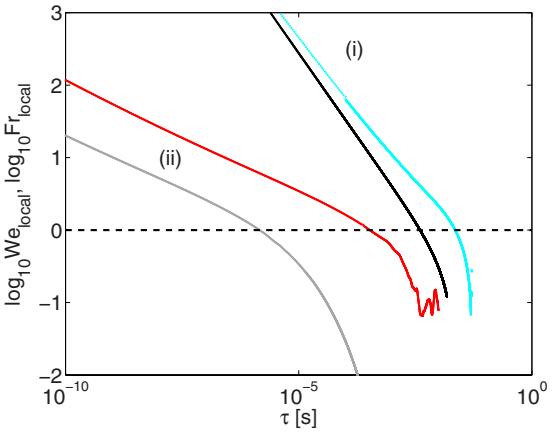

FIG. 6. (Color online) The local Froude number for system (i) and an impact Froude number Fr=3.4 (cyan, rightmost curve) and Fr=4000 (black) and the local Weber number for system (ii) with configuration A (red, dark gray) and B (gray, leftmost curve). The onset of the universal regime can be located roughly after the respective nondimensional quantities have become larger than order unity (horizontal dashed line).

At the same time the distance between the two disk impacts with Fr=3.4 and Fr=4000 is smaller than that between the two needle setups A and B. Accordingly, the duration of the universal regime varies only between ~1 and ~6 ms for the disk, while in the needle setup it depends much stronger on initial conditions varying from microseconds down to several nanoseconds as seen above.

We will now explain the Froude dependence of the experimentally and numerically observed exponents in [4] for the impacting disk. Based on Fig. 5(a) these exponents can be viewed as a time average of the local exponent. Due to the limited resolution and the onset of other effects (e.g., air flow) only the right part of these plots is accessible in experiments and the time average will be heavily weighted toward the beginning of the universal regime, i.e., to a region just around and left of the maximum in Fig. 5(a). We can thus assume the experimentally observed effective exponent to be roughly equal to the maximum value of the local exponent, which is where the universal behavior sets in. As can be seen in Fig. 5(a) the approach to the maximum is almost vertical, which implies that γ remains constant during a certain time before pinch. This allows us to approximate the aspect ratio where universality is reached by the macroscopic aspect ratio γ_i of the cavity at the start of the universal regime. Using Eq. (2) we can predict this value once the characteristic initial aspect ratio γ_i for each cavity is known.

This quantity γ_i however is not straightforward to determine since the configuration before impact is simply a flat surface and the only value available to characterize the initial conditions is the Froude number. We are nevertheless able to provide an estimate for γ_i as illustrated in Fig. 7(a) which shows the cavity shape at the beginning of the universal

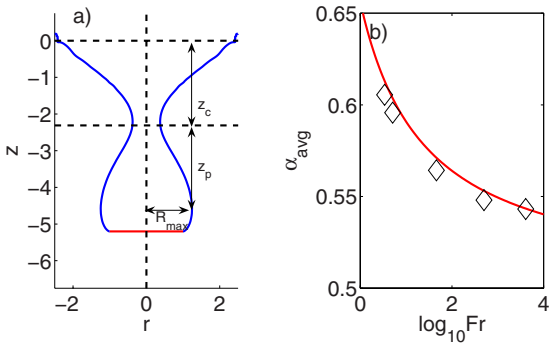

FIG. 7. (Color online) (a) Illustration of the characteristic aspect ratio of the cavity. (b) The averaged exponent measured in [4] (black diamonds) is reproduced very well by our model with the constant $K=0.46$ (red line).

regime. The horizontal size of this cavity is its maximum radial expansion $R_{\max}$. The characteristic vertical length scale can be assumed to be proportional to the depth of eventual closure z_c. For both quantities the dependence on initial conditions can be written in terms of scaling laws with the impact Froude number. The horizontal length scales approximately as $R_{\max} \sim \mathrm{Fr}^{1/4}$ [14], while the vertical length behaves as $z_c \sim \mathrm{Fr}^{1/2}$ [14,30].

With these two quantities in hand we can estimate the characteristic initial aspect ratio as

$$\gamma_i = C\frac{R_{\max}}{z_c} \approx 2K^{-1/4}\,\mathrm{Fr}^{-1/4} \tag{3}$$

with C and K constants of order unity. Inserting this γ_i into Eq. (2) and solving for $\alpha(\mathrm{Fr})$, again neglecting $d\alpha/d\ln\tau$, gives

$$\alpha = \frac{\ln(K\,\mathrm{Fr})}{2\ln(K\,\mathrm{Fr}) - 2}. \tag{4}$$

We can thus predict the experimentally observable averaged exponent, which is found in excellent agreement with [4] as demonstrated by Fig. 7(b). Thus, the way how the experimentally and numerically observed exponents depend on the global impact parameters [4] constitutes an impressive manifestation of universal behavior in this system.

In conclusion, we have demonstrated that the universal theory of [12,27] faithfully predicts the approach of the neck radius for inviscid axisymmetric bubble pinch-off in four different systems widely studied in the literature over the past years. Remarkably, however, the duration of the final regime is shown to be strongly dependent on the type of the system and on the various control parameters employed. While it lies easily within experimentally accessible time scales (~ms) for an impacting circular disk, it can be as low as a few nanoseconds for gas bubbles injected through a small orifice into a quiescent liquid pool. We were able to trace this difference back to the relative importance of the respective driving forces. Our findings reconcile the prediction of universality in bubble pinch-off [11,12] with an apparent dependence on initial conditions [4], an apparently constant scaling exponent [5,6,8], and with the observation that noninertial forces can be dominant in many experimental settings [9,10,20].

This work is part of the program of the Stichting FOM, which is financially supported by NWO.

[1] M. S. Longuet-Higgins, B. R. Kerman, and K. Lunde, J. Fluid Mech. **230**, 365 (1991).
[2] H. N. Oguz and A. Prosperetti, J. Fluid Mech. **257**, 111 (1993).
[3] J. M. Gordillo, A. Sevilla, J. Rodríguez-Rodríguez, and C. Martínez-Bazán, Phys. Rev. Lett. **95**, 194501 (2005).
[4] R. Bergmann, D. van der Meer, M. Stijnman, M. Sandtke, A. Prosperetti, and D. Lohse, Phys. Rev. Lett. **96**, 154505 (2006).
[5] N. C. Keim, P. Møller, W. W. Zhang, and S. R. Nagel, Phys. Rev. Lett. **97**, 144503 (2006).
[6] S. T. Thoroddsen, T. G. Etoh, and K. Takehara, Phys. Fluids **19**, 042101 (2007).
[7] J. M. Gordillo, A. Sevilla, and C. Martínez-Bazán, Phys. Fluids **19**, 077102 (2007).
[8] J. C. Burton and P. Taborek, Phys. Rev. Lett. **101**, 214502 (2008).
[9] J. M. Gordillo, Phys. Fluids **20**, 112103 (2008).
[10] R. Bolaños-Jiménez, A. Sevilla, C. Martinez-Bazán, and J. M. Gordillo, Phys. Fluids **20**, 112104 (2008).
[11] J. M. Gordillo and M. Pérez-Saborid, J. Fluid Mech. **562**, 303 (2006).
[12] J. Eggers, M. A. Fontelos, D. Leppinen, and J. H. Snoeijer, Phys. Rev. Lett. **98**, 094502 (2007).
[13] J. Eggers, Rev. Mod. Phys. **69**, 865 (1997).
[14] R. Bergmann, D. van der Meer, S. Gekle, A. van der Bos, and D. Lohse, J. Fluid Mech. **633**, 381 (2009).
[15] J. C. Burton, R. Waldrep, and P. Taborek, Phys. Rev. Lett. **94**, 184502 (2005).
[16] L. E. Schmidt, N. C. Keim, W. W. Zhang, and S. R. Nagel, Nat. Phys. **5**, 343 (2009).
[17] K. S. Turitsyn, L. Lai, and W. W. Zhang e-print arXiv:0902.0393v1.
[18] S. Gekle, J. M. Gordillo, D. van der Meer, and D. Lohse, Phys. Rev. Lett. **102**, 034502 (2009).
[19] J. Rodríguez-Rodríguez, J. M. Gordillo, and C. Martínez-Bazán, J. Fluid Mech. **548**, 69 (2006).
[20] J. M. Gordillo and M. A. Fontelos, Phys. Rev. Lett. **98**, 144503 (2007).
[21] D. Leppinen and J. Lister, Phys. Fluids **15**, 568 (2003).
[22] M. Nitsche and P. H. Steen, J. Comput. Phys. **200**, 299 (2004).
[23] R. Bergmann, A. Andersen, D. van der Meer, and T. Bohr, Phys. Rev. Lett. **102**, 204501 (2009).
[24] S. Gekle, A. van der Bos, R. Bergmann, D. van der Meer, and D. Lohse, Phys. Rev. Lett. **100**, 084502 (2008).

[25] See EPAPS Document No. E-PLEEE8-80-009909 for supplementary material. For more information on EPAPS, see http://www.aip.org/pubservs/epaps.html.

[26] A Taylor expansion of the cavity profile around the neck yields $r(z)=r_0+(\partial^2 r/\partial z^2)\Delta z^2/2=r_0+(1/r_c)(\Delta z^2/2)$. To collapse these profiles one can rescale the radial length scale with $r'=r/r_0$ and the axial length scale with $z'=z/\sqrt{r_0 r_c}$ to obtain the time-independent shape $r'=1+\Delta z'^2/2$.

[27] M. A. Fontelos, J. H. Snoeijer, and J. Eggers (unpublished).

[28] In the BI data we verified that $|d\alpha/d \ln \tau| \ll |\alpha-2\alpha^2|$.

[29] The long duration of the universal regime for the quasistatic case A can be understood as follows: in case A the maximum diameter of the bubble is only slightly larger than the orifice in contrast to the other two situations where the bubble is much larger than the needle exit. Accordingly, the neck in case A possesses already initially a rather symmetrical shape with its upper half being very similar to the lower one, which is prerequisite for the universal solution to be applicable.

[30] V. Duclaux, F. Caillé, C. Duez, C. Ybert, L. Bocquet, and C. Clanet, J. Fluid Mech. **591**, 1 (2007).